

Article

# Unexpected Synthesis, Single-Crystal X-ray Structure, Anticancer Activity, and Molecular Docking Studies of Certain 2-((Imidazole/Benzimidazol-2-yl)thio)-1-arylethanones

Tarfah Al-Warhi <sup>1</sup>, Mohamed A. Said <sup>2</sup>, Mahmoud A. El Hassab <sup>3</sup> , Nada Aljaeed <sup>1</sup>, Hazem A. Ghabour <sup>4</sup> , Hadia Almahli <sup>5,6</sup>, Wagdy M. Eldehna <sup>7,\*</sup>  and Hatem A. Abdel-Aziz <sup>8,\*</sup> 

<sup>1</sup> Department of Chemistry, College of Science, Princess Nourah bint Abdulrahman University, Riyadh 11671, Saudi Arabia; tarfah-w@hotmail.com (T.A.-W.); noaljaeed@pnu.edu.sa (N.A.)

<sup>2</sup> Department of Pharmaceutical Chemistry, Faculty of Pharmacy, Egyptian Russian University, Badr City 11829, Cairo, Egypt; madyyy\_@hotmail.com

<sup>3</sup> Department of Pharmaceutical Chemistry, School of Pharmacy, Badr University in Cairo, Badr City 11829, Cairo, Egypt; elhasabma85@gmail.com

<sup>4</sup> Department of Medicinal Chemistry, Faculty of Pharmacy, Mansoura University, Mansoura 35516, Egypt; ghabbourh@yahoo.com

<sup>5</sup> Department of Chemistry, Chemistry Research Laboratory, University of Oxford, 12 Mansfield Road, Oxford OX1 3TA, UK; hadia.almahli@yahoo.com

<sup>6</sup> Department of Chemistry, School of Life Sciences, University of Sussex, Sussex House, Falmer, Brighton BN1 9RH, UK

<sup>7</sup> Department of Pharmaceutical Chemistry, Faculty of Pharmacy, Kafrelsheikh University, Kafrelsheikh 33516, Egypt

<sup>8</sup> Department of Applied Organic Chemistry, National Research Center, Dokki, Giza, P.O. Box 12622, Egypt

\* Correspondence: wagdy2000@gmail.com (W.M.E.); hatem\_741@yahoo.com (H.A.A.-A.)

Received: 29 April 2020; Accepted: 25 May 2020; Published: 31 May 2020



**Abstract:** In connection with our research program concerning development of novel effective benzimidazole-based anticancer candidates, herein we describe a new unexpected synthetic route to obtain a series of 2-((imidazole/benzimidazol-2-yl)thio)1-arylethanones endowed with promising anti-breast cancer and Cyclin-dependent kinase 2 (CDK2) inhibitory activities. Contrary to expectations, products for the reaction of 2-mercaptoimidazole/benzimidazole 2a,b with  $\beta$ -keto esters 6a–c were unambiguously assigned as 2-((imidazol/benzimidazol-2-yl)thio)1-arylethanones 10a–f based on NMR spectroscopy and single-crystal X-ray crystallographic analyses. In vitro anticancer activities for herein reported imidazole/benzimidazoles 10a–f were assessed through a cell-based assay against human breast cancer T4–7D and MCF–7 cell lines. Benzimidazoles 10d–f exerted better anti-proliferative action towards T4–7D and MCF–7 cell lines than their corresponding imidazole counterparts 10a–c. Furthermore, a molecular docking study suggested CDK2 kinase as a potential enzymatic target for benzimidazoles 10d–f, and investigated their possible binding pattern and interactions within CDK2 active site. Thereafter, benzimidazoles 10d–f were in vitro examined for their CDK2 inhibitory action, where they exerted good activity. Finally, several key ADME and druglikeness properties were predicted by the SwissADME online tool. Interestingly, benzimidazoles 10d–f were found to have no violations in all druglikeness rules (Veber, Lipinski, Ghose, Muegge, and Egan). In addition, they had neither PAINS nor structural alerts (Brenks). In conclusion, benzimidazoles 10d–f demonstrated not only a promising anticancer activities but also an acceptable ADME and physicochemical properties especially benzimidazole 10e.

**Keywords:** imidazole/benzimidazole;  $\beta$ -keto esters; anticancer; cdk2 inhibitors; single-crystal X-ray analyses

## 1. Introduction

On account of their existence in several natural bioactive compounds and some naturally occurring nucleotides in addition to their significant roles as therapeutics in diverse clinical applications, imidazole and benzimidazole are occupying a featured position in the synthetic medicinal chemistry [1–4].

Imidazoles and benzimidazoles are quite unique and universally privileged scaffolds, which are core units in numerous drugs and drug candidates [5] such as angiotensin II receptor antagonists,  $H^+/K^+$ -ATPases inhibitors,  $H_1$ -antihistamines, anthelmintics, and anticancer agents. Accordingly, medicinal chemists embarked on developing and exploring varied imidazole- and benzimidazole-based small molecules to afford novel and promising biologically active compounds. In this context, imidazoles and benzimidazoles emerged as important structural motifs for anticancer drug discovery and development with diverse potential cellular and enzymatic targets [6–10].

In recent years, there are several innovative, efficient, and mild synthetic protocols and routes that have been reported for the development of benzimidazole-based small molecules. Some studies reported the synthesis of benzimidazoles by the use of water as the reaction medium [11,12]. In addition, many other green synthetic methods have been reported [13–15]. Moreover, a large number of studies utilized different catalysts to synthesize diverse benzimidazole derivatives [16], to name just a few, the palladium-catalyzed [17], zinc-catalyzed [18], erbium-catalyzed [14], and copper-catalyzed synthesis [19].

In the last few years, we have reported two studies to investigate the antitumor actions for a series of 23 2-((benzimidazol-2-yl)thio)-1-arylethanone derivatives (structures 1, Figure 1) through different cell-based assays [20,21]. The first study revealed the capability of these benzimidazole derivatives to affect the bulk of tumor cells and cancer stem cells via inhibition of growth of the HT29 colon cancer cells and the CD133 cell-surface expression, a cancer stem cell marker, in HT29 cells [20]. In the second study, the explored benzimidazole derivatives 1 (Figure 1) displayed promising anticancer action toward triple-negative MDAMB4–68 breast cancer cell line, in addition to induction of apoptosis in the same cells. In both previous studies, the target benzimidazole derivatives 1 were prepared through reaction of 2-mercaptobenzimidazole 2b,  $R = -(CH_2)_4$ , with different acetophenones in boiling glacial acetic acid and two equivalents of concentrated sulfuric acid, with sequent neutralization for the produced sulfate salts yielding 2-((benzimidazol-2-yl)thio)-1-arylethanones 3 in a good yield [20,21] (Figure 1).

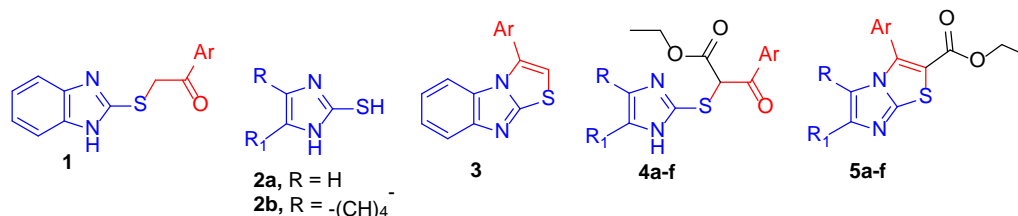
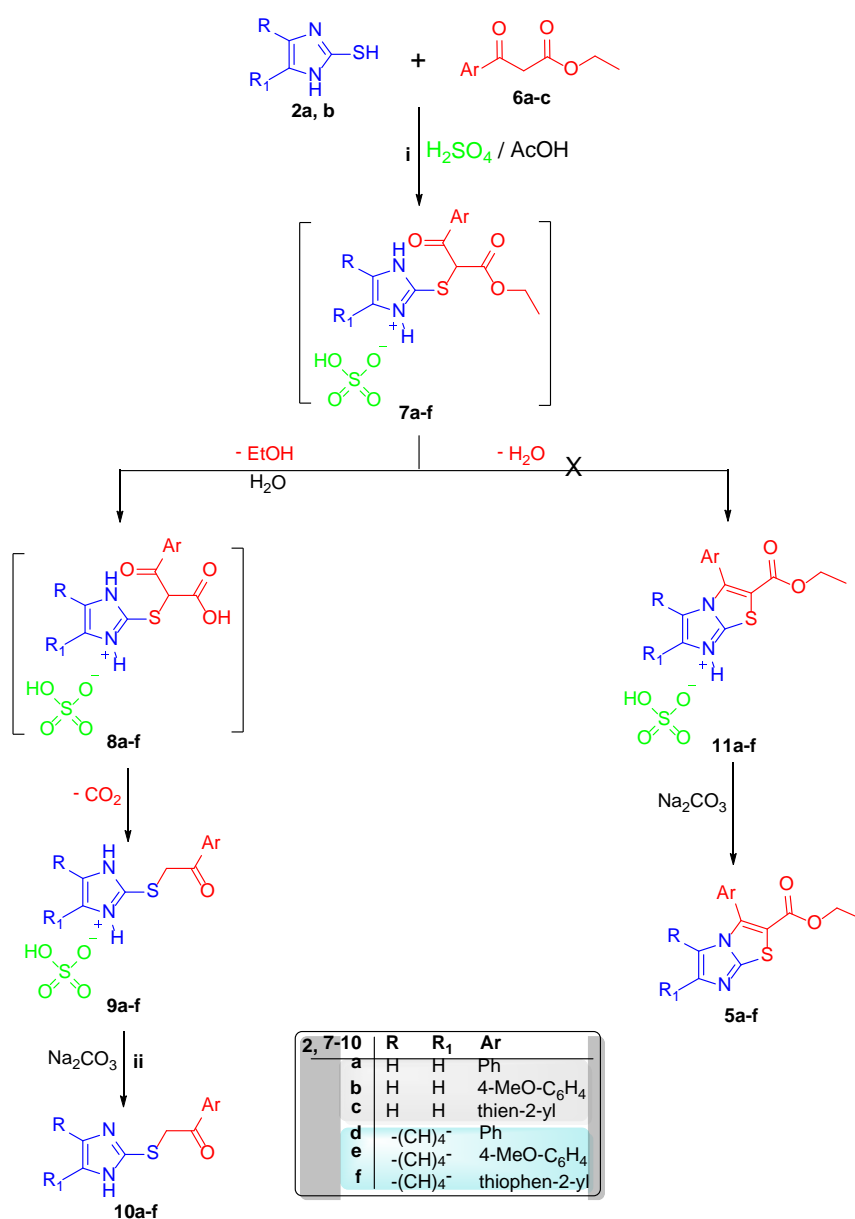


**Figure 1.** Chemical structure of compounds 1–5.

In 2017, we reported another study that adopted a structural rigidification approach to develop new set of 3-arylthiazolo[3,2-*a*]benzimidazole derivatives (structure 3, Figure 1) as rigid analogues to the previously reported 2-((benzimidazol-2-yl)thio)-1-arylethanones 1 [22]. The prepared arylthiazolo[3,2-*a*]benzimidazole derivatives exerted efficient growth-inhibitory action against triple-negative MDAMB4–68 breast cancer and HT29 colon cancer cell lines in addition to their capability to inhibit the CD133 cell surface expression. This arylthiazolo[3,2-*a*]benzimidazole series

was prepared through a one-pot, two-components heterocyclization reaction, via the reaction of 2-mercaptobenzimidazole **2b** with different acetophenones in boiling glacial acetic acid and five equivalents from concentrated sulfuric acid [22].

Based on the reported effective antitumor activities for both 2-((benzimidazol-2-yl)thio)1-arylethanones (**1**) as well as 3-arylthiazolo[3,2-*a*]benzimidazole derivatives (**3**) series [20–22], in the current research work we aspired to develop a novel series of imidazole/benzimidazole-based esters **4** and their cyclized analogues **5** (Figure 1) via the reaction of imidazole/benzimidazole thiols **2a,b** with different  $\beta$ -keto esters in boiling glacial acetic acid, in the presence of two and five equivalents of concentrated sulfuric acid, respectively, following the above-mentioned procedure [20–22]. Interestingly, this reaction afforded an unexpected sulfate salts **9** (Scheme 1) rather than sulfate salts for **4** or **5**. The latter sulfate salts **9** were then neutralized to produce 2-((benzimidazol-2-yl)thio)1-arylethanones **10** (Scheme 1). This reaction, as well as its proposed pathway, will be discussed in this study in the light of X-ray single-crystal analysis for **9b** and **10f**.



**Scheme 1.** Reaction of imidazole/benzimidazole thiols **2a, b** with  $\beta$ -keto esters **6a–c** (i) reflux for 1 h, (ii) stirring at room temperature for 3 h.

Moreover, the anticancer activities for herein-reported imidazole/benzimidazole derivatives 10a–f will be assessed through a cell-based assay (against human breast cancer T4–7D and MCF–7 cell lines) as well as through a cell-free assay (against Cyclin-dependent kinase 2, CDK2) to explore the potential enzymatic targets for the prepared derivatives 10a–f. Also, several key physicochemical parameters will be calculated in order to explore their pharmacokinetics and druglikeness properties.

## 2. Results and Discussion

### 2.1. Chemistry

This study describes the reaction of 2-mercaptoimidazole (2a) and 2-mercaptobenzimidazole (2b) with  $\beta$ -keto esters 6a–c in an attempt to obtain a new series of ethyl 2-((imidazol/benzimidazol2-yl)thio)3-oxo3-arylpropanoates 4a–f or ethyl 3-aryl imidazol/benzimidazo[2,1-*b*]thiazole2-carboxylates 5a–f (Scheme 1). The expected synthetic pathway for this reaction is depicted in Scheme 1. The conditions adopted for this reaction were heating under reflux in acetic acid and in the existence of two equivalents from  $H_2SO_4$  (98%) followed by neutralization with sodium bicarbonate, which is similar to the reported conditions in our previous studies for the reaction of 2-mercaptobenzimidazole with different acetophenones [20,21].

As shown in Scheme 1, contrary to expectations, the products were unambiguously assigned as 2-((imidazol/benzimidazol2-yl)thio)1-arylethanones 10a–f instead of ethyl 2-((imidazol/benzimidazol2-yl)thio)3-oxo3-arylpropanoates 4a–f or ethyl 3-aryl imidazol/ benzimidazo[2,1-*b*]thiazole2-carboxylates 5a–f, based on NMR spectroscopy and X-ray crystallographic analysis of sulfate salt 9b and free base 10f (Scheme 1). The analytical data and physical characters of products 9d–f and 10d–f were similar to the products afforded from the reaction of the corresponding acetophenones with 2-mercapto-imidazole/benzimidazole 2a,b under the same reaction conditions (Scheme 1).

The proposed reaction pathway for this unexpected manner was suggested, as in Scheme 1, that an electrophilic attack between 2-mercaptoimidazole (2a) or 2-mercaptobenzimidazole (2b) and the alpha carbon of  $\beta$ -keto esters 6a–c took place, forming 2-((1-ethoxy1-, 3-dioxo3-arylpropan2-yl)thio)1-*H*-imidazol/benzimidazol3-ium hydrogen sulfate salts 7a–f. These salt intermediates were subjected to ester hydrolysis, affording the corresponding acid intermediates 8a–f, respectively, that subsequently decarboxylated to produce the salt products 9a–f. Neutralization of sulfate salts 9a–f was performed via stirring with an aqueous solution of sodium hydrogen carbonate in order to yield 10a–f, respectively (Scheme 1).

The  $^1H$  NMR spectra for imidazol/benzimidazoles 10a–f confirmed disappearance of the triplet and quartet signals attributable to the aliphatic protons in the ethyl ester functionality ( $-COOCH_2CH_3$ ). In addition, they displayed the alpha-protons as singlet signals integrated for two protons of  $-S-CH_2-$ . Furthermore,  $^{13}C$  NMR spectra for imidazole/benzimidazole-based derivatives 10a–f uncovered the disappearance of the carbons of the ethyl ester group ( $-COOCH_2CH_3$ ). Moreover, the single-crystal X-ray analysis was utilized to confirm the structure of compounds 9b and 10f unambiguously.

### 2.2. Single-Crystal X-ray Crystallographic Analysis

Crystallographic data for imidazole sulfate-salt 9b and benzimidazole derivative 10f were assigned CCDC numbers 1524590 and 1429947, respectively, in the Cambridge Crystallographic Data Centre. The asymmetrical unit of imidazole sulfate-salt 9b contained one molecule cation and one hydrogen sulfate anion to form a stable salt, Figure 2. Regarding benzimidazole derivative 10f, the unit cell contained only one independent base molecule. The bond lengths, as well as angles, were in the normal ranges [23]. Molecules of imidazole sulfate-salt 9b were linked via five intermolecular hydrogen bonds in order to build a network structure (Figure 3) in the crystal packing. On the other hand, benzimidazole derivative 10f was packed together through one strong hydrogen bond along the *b* axis (Figure 4). Certain chosen bond lengths and angles, as well as hydrogen bond geometry of compounds 9b and 10f, are listed in Tables 1 and 2, respectively.

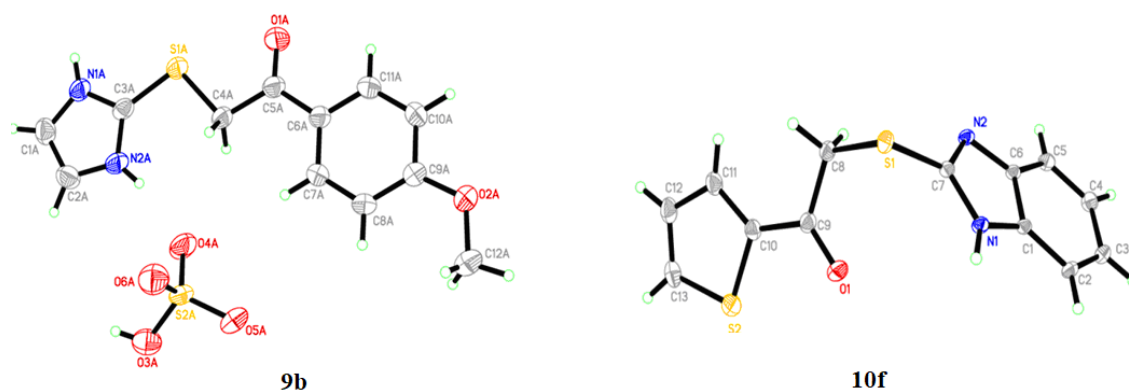


**Figure 2.** Oak Ridge Thermal Ellipsoid Plot (ORTEP) diagrams for imidazole sulfate-salt **9b** and benzimidazole derivative **10f**. Displacement ellipsoids have been plotted at the 40% probability level for non-H atoms.

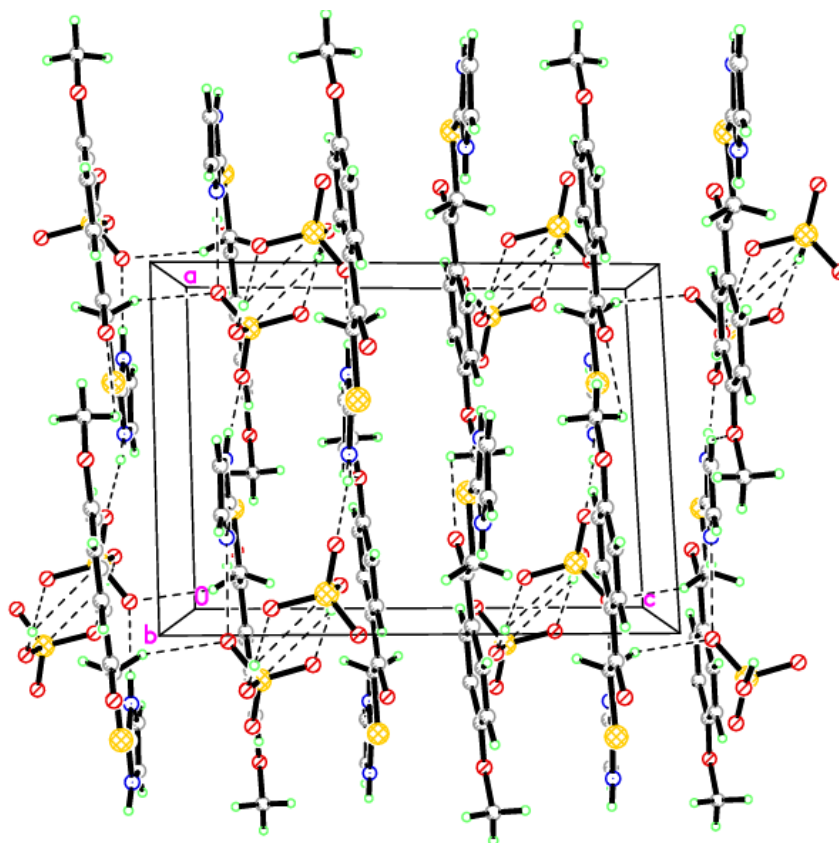


**Figure 3.** Molecular packing for imidazole sulfate-salt **9b**, showing hydrogen bonds that were drawn as dashed lines forming a network structure.

### 2.3. Biological Evaluation

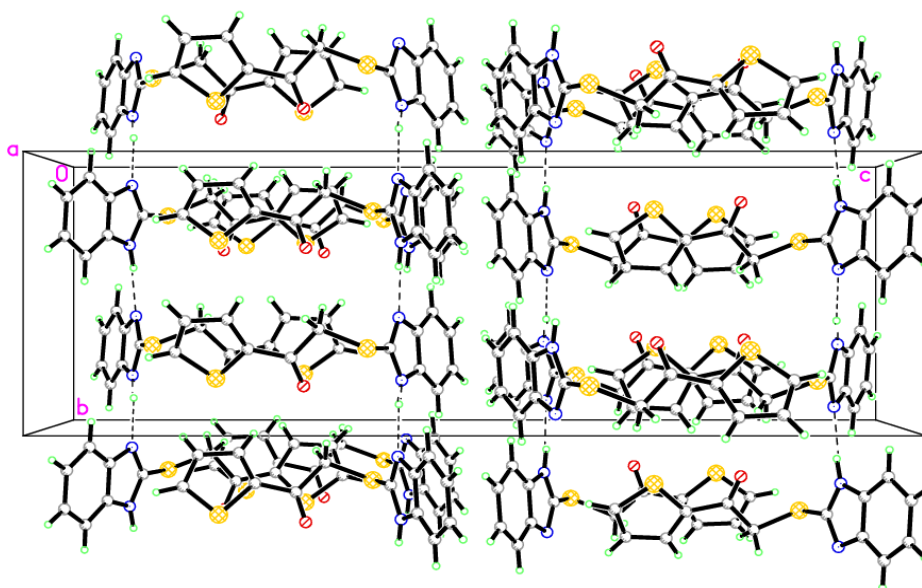
#### Cytotoxic Action against Breast Cancer Cell Lines

The potential anti-proliferative action toward two human breast cancer cell lines, T4-7D and MCF-7, was assessed for all the synthesized imidazole derivatives (10a–c) and benzimidazole derivatives (10d–f) by the aid of Sulforhodamine B (SRB) assay [24] where the approved antitumor drug staurosporine was incorporated as a positive control in the experiments. The calculated  $IC_{50}$  values (a concentration demanded to inhibit proliferation of the tumor cells by 50%) are displayed in Table 3.

**Table 1.** Selected geometric parameters (Å, °) of imidazole sulfate-salt **9b** and benzimidazole derivative **10f**.

<b>9b</b>			
<b>Bond</b>	<b>Å</b>	<b>Bond</b>	<b>Å</b>
S1A—C3A	1.732(2)	O2A—C12A	1.428(3)
S1A—C4A	1.807(2)	O2A—C9A	1.354(3)
S1B—C4B	1.805(2)	O1B—C5B	1.208(3)
S1B—C3B	1.729(2)	O2B—C12B	1.433(3)
S2A—O4A	1.4343(19)	O2B—C9B	1.357(3)
S2A—O3A	1.5235(19)	N1A—C3A	1.324(3)
S2A—O5A	1.4346(18)	N1A—C1A	1.376(3)
S2A—O6A	1.4764(18)	N2A—C2A	1.370(3)
S2B—O4B	1.5283(17)	N2A—C3A	1.332(3)
S2B—O5B	1.4782(18)	N1B—C3B	1.326(3)
S2B—O6B	1.4330(18)	N1B—C1B	1.379(3)
S2B—O3B	1.4346(17)	N2B—C2B	1.372(3)
O1A—C5A	1.212(3)	N2B—C3B	1.329(3)
<b>Angle</b>	<b>°</b>	<b>Angle</b>	<b>°</b>
C3A—S1A—C4A	99.79(10)	N1A—C1A—C2A	106.5(2)
C3B—S1B—C4B	99.33(10)	N2A—C2A—C1A	107.5(2)
O4A—S2A—O5A	112.49(11)	N1A—C3A—N2A	107.11(19)
O4A—S2A—O6A	111.10(11)	S1A—C3A—N1A	122.50(16)
O3A—S2A—O6A	106.18(10)	S1A—C3A—N2A	130.35(16)
O5A—S2A—O6A	111.22(11)	S1A—C4A—C5A	106.53(14)
O3A—S2A—O4A	109.48(11)	O1A—C5A—C6A	122.4(2)
O3A—S2A—O5A	106.04(11)	O1A—C5A—C4A	119.07(19)
O2A—C9A—C8A	125.06(18)	O2A—C9A—C10A	115.36(19)
<b>10f</b>			
<b>Bond</b>	<b>Å</b>	<b>Bond</b>	<b>Å</b>
S1—C7	1.7515(12)	N1—C1	1.3752(16)
S1—C8	1.8058(13)	N1—C7	1.3554(15)
S2—C10	1.7236(13)	N2—C6	1.3865(15)
S2—C13	1.7082(16)	N2—C7	1.3224(15)
O1—C9	1.2162(18)		
<b>Angle</b>	<b>°</b>	<b>Angle</b>	<b>°</b>
C7—S1—C8	100.47(6)	N1—C7—N2	113.39(10)
C10—S2—C13	91.62(7)	S1—C7—N1	121.61(8)
C1—N1—C7	106.66(9)	S1—C8—C9	113.44(9)
C6—N2—C7	104.82(9)	O1—C9—C10	121.54(12)
N1—C1—C2	131.98(11)	O1—C9—C8	122.19(11)
N1—C1—C6	105.79(10)	S2—C10—C11	111.21(10)
N2—C6—C1	109.33(10)	S2—C10—C9	119.21(10)
N2—C6—C5	130.19(10)	S2—C13—C12	112.46(11)
S1—C7—N2	124.83(9)		

The tested imidazole and benzimidazole derivatives displayed different levels of growth-inhibitory action toward the examined two breast cancer T4-7D and MCF-7 cell lines. As can be seen in Table 3, the tested imidazole/benzimidazole derivatives were more potent against MCF-7 cell line ( $IC_{50}$  range:  $4.53 \pm 0.33 - 72.64 \pm 4.05 \mu\text{M}$ ) than T4-7D cell line ( $IC_{50}$  range:  $8.04 \pm 0.32 - >100 \mu\text{M}$ ), with an exception for benzimidazole derivative 10d that displayed enhanced activity against T4-7D cell line ( $IC_{50} = 8.04 \pm 0.32 \mu\text{M}$ ) than MCF-7 cell line ( $IC_{50} = 12.90 \pm 1.04 \mu\text{M}$ ).

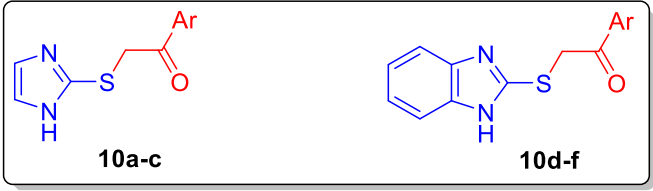


**Figure 4.** Molecular packing for benzimidazole **10f**, showing hydrogen bonds that were drawn as dashed lines along the *b* axis.

**Table 2.** Hydrogen-bond geometry (Å, °) for **9b** and **10f**.

<b>9b</b>				
<i>D—H...A</i>	<i>D—H</i>	<i>H...A</i>	<i>D...A</i>	<i>D—H...A</i>
O3A—H3AA...O5B	0.8200	1.8300	2.648(3)	180.00
O4B—H4BC...O6A	0.8200	1.8200	2.635(3)	179.00
N2B—H2NB...O6B <sup>i</sup>	0.77(3)	2.04(3)	2.805(3)	172(2)
N2A—H2NA...O4A	0.80(3)	1.98(3)	2.762(3)	168(2)
N1A—H1NA...O5A <sup>i</sup>	0.81(3)	1.96(3)	2.769(3)	173(3)
N1B—H1NB...O3B	0.83(3)	1.94(3)	2.768(2)	173(2)
C1A—H1AA...O2A <sup>ii</sup>	0.9300	2.5400	3.259(3)	134.00
C1B—H1BA...O2B <sup>iii</sup>	0.9300	2.5400	3.274(3)	136.00
C4B—H4BA...O6B <sup>iv</sup>	0.9700	2.5000	3.423(3)	158.00
Symmetry codes: (i) $x + 1, y, z$ ; (ii) $x + 1, y + 1, z$ ; (iii) $x - 1, y - 1, z$ ; (iv) $-x + 1, -y + 1, -z + 2$ ; (v) $x - 1, y, z$ .				
<b>10f</b>				
<i>D—H...A</i>	<i>D—H</i>	<i>H...A</i>	<i>D...A</i>	<i>D—H...A</i>
N1—H1N1...N2 <sup>i</sup>	0.906(19)	1.88(2)	2.7858(14)	173.7(16)
Symmetry code: (i) $-x + 1/2, y + 1/2, z$ .				

As for the growth-inhibitory action against MCF-7 cell line, benzimidazole derivative **10e** was the most efficient analogue in the current study possessing better efficiency ( $IC_{50} = 4.53 \pm 0.33 \mu\text{M}$ ) than reference drug staurosporine ( $IC_{50} = 6.67 \pm 0.28 \mu\text{M}$ ) (Table 3). In addition, compound **10d** displayed good activity toward MCF-7 cells ( $IC_{50} = 12.90 \pm 1.04 \mu\text{M}$ ) that represent two-fold decreased efficiency than staurosporine ( $IC_{50} = 6.67 \pm 0.28 \mu\text{M}$ ). In addition, imidazole derivatives **10a** and **10b** and benzimidazole derivative **10f** possessed moderate growth-inhibitory action toward MCF-7 cell line with  $IC_{50}$  values equal to  $42.61 \pm 3.08$ ,  $31.25 \pm 2.36$ , and  $23.07 \pm 2.19 \mu\text{M}$ , respectively, whereas, imidazole derivative **10c** exhibited weak cytotoxic action toward MCF-7 cells ( $IC_{50} = 6.67 \pm 0.28 \mu\text{M}$ ).

**Table 3.** In vitro anticancer activity of imidazole derivatives (10a–c) and benzimidazole derivatives (10d–f) against breast cancer T4–7D and MCF–7 cell lines.


Cpd.	Ar	IC <sub>50</sub> (μM) <sup>a</sup>	
		T-47D	MCF-7
10a	C <sub>6</sub> H <sub>5</sub>	57.68 ± 0.25	42.61 ± 3.08
10b	4-CH <sub>3</sub> O-C <sub>6</sub> H <sub>4</sub>	39.32 ± 0.08	31.25 ± 2.36
10c	thien2-yl	NA <sup>b</sup>	72.64 ± 4.05
10d	C <sub>6</sub> H <sub>5</sub>	8.04 ± 0.32	12.90 ± 1.04
10e	4-CH <sub>3</sub> O-C <sub>6</sub> H <sub>4</sub>	11.17 ± 0.04	4.53 ± 0.33
10f	thien-2-yl	34.94 ± 0.37	23.07 ± 2.19
Staurosporine	–	7.19 ± 0.43	6.67 ± 0.28

<sup>a</sup> IC<sub>50</sub>s calculated as the mean ± SD of three separate experiments. <sup>b</sup> NA: Compound showing IC<sub>50</sub> value more than 100 μM.

With regard to the anticancer activity toward breast cancer T4–7D cell line, benzimidazole derivative 10d emerged as the best counterpart in inhibiting growth of the T4–7D cells with comparable activity (IC<sub>50</sub> = 8.04 ± 0.32 μM) to reference drug staurosporine (IC<sub>50</sub> = 7.19 ± 0.43 μM), Table 3. Besides, benzimidazole derivative 10e efficiently inhibited growth of the T4–7D cells with IC<sub>50</sub> value equal to 11.17 ± 0.04 μM. Moreover, T4–7D cell line was moderately affected by imidazole derivatives 10a and 10b and benzimidazole derivative 10f (IC<sub>50</sub> = 34.94 ± 0.37, 57.68 ± 0.25 and 39.32 ± 0.08 μM, respectively), whereas, imidazole derivative 10c failed to inhibit the growth of the examined T4–7D cells up to 100 μM.

Certain structure activity relationships (SARs) should be highlighted from the obtained results (Table 3). Utilization of the benzimidazole scaffold was suggested to be more beneficial for the anticancer activity as evidenced by the enhanced anti-proliferative action of benzimidazole derivatives 10d–f towards both T4–7D (IC<sub>50</sub> = 8.04 ± 0.32, 11.17 ± 0.04 and 34.94 ± 0.37 μM, respectively) and MCF–7 cell lines (IC<sub>50</sub> = 12.90 ± 1.04, 4.53 ± 0.33 and 23.07 ± 2.19 μM, respectively) than their corresponding imidazole counterparts 10a–c (T4–7D; IC<sub>50</sub> = 57.68 ± 0.25, 39.32 ± 0.08 and > 100 μM, respectively) (MCF–7; IC<sub>50</sub> = 42.61 ± 3.08, 31.25 ± 2.36 and 72.64 ± 4.05 μM, respectively). Another aspect worth mentioning is that bioisosteric replacement for the pendant phenyl ring with the heterocyclic thiophene, within the imidazole and benzimidazole derivatives, led to dramatic decrease or even abolishment of activity towards the two examined breast cancer T4–7D and MCF–7 cell lines. Moreover, *para*-substitution of the phenyl ring in compounds 10a and 10d (IC<sub>50</sub> = 42.61 ± 3.08 and 12.90 ± 1.04 μM, respectively) with the electron-donating methoxy group resulted in compounds 10b and 10e with enhanced anticancer activity against MCF–7 cell line (IC<sub>50</sub> = 31.25 ± 2.36 and 4.53 ± 0.33 μM, respectively).

## 2.4. CDK Inhibitory Action

### 2.4.1. CDK Molecular Modeling

On account of their promising anticancer actions toward the two tested human breast cancer T4–7D and MCF–7 cell lines, benzimidazole derivatives 10d–f were selected to be further investigated for their potential mechanism of action.

First, molecular modeling study was conducted to explore the potential binding interactions and energy scores within CDK2, CDK4/6, CDK7, and CDK9 kinases' active sites.

The crystal structures of CDK2, CDK4/6, CDK7, and CDK9 were obtained from the Protein Data Bank, PDB IDs: 5EIV [25], 5I2i [26], 1ua2 [27], and 3lq5 [28], respectively).

In drug design, docking is an inventible technique that enables the prediction of binding between ligand and receptor and is very useful in interpretation of the biological data. However, docking is an error-prone technique and must be validated. Thus, the four co-crystallized ligands in the enzymes were re-docked to their corresponding enzymes and the Root-mean-square deviation (RMSD) values between the docked and co-crystallized ligands were less than 0.6 in both the NW-docking (docking without water) and W-docking (docking with water) (Table S1). The obtained results indicated a reliable docking protocol and guided us to remove the water molecules [29]. In particular, compounds 10d–f achieved a good, acceptable binding affinity only against CDK2 with compound 10e achieving the highest score,  $-8.9$  Kcal/mole, while compounds 10d and 10f achieved  $-8.7$  and  $-8.0$  Kcal/mole, respectively (Table 4). Accordingly, the  $IC_{50}$  values will be determined against CDK2.

**Table 4.** Docking energy scores in kcal/mol (*S*) for benzimidazoles 10d–f.

Cpd.	Energy Score ( <i>S</i> ) kcal/mol			
	CDK2	CDK4/6	CDK7	CDk9
10d	$-8.7$	$-7.2$	$-6.6$	$-7.3$
10e	$-8.9$	$-7.2$	$-6.7$	$-7.5$
10f	$-8.0$	$-6.7$	$-6.5$	$-7.0$

Generally, CDK2 has a hydrophobic active site consisting of nonpolar amino acids like valine, leucine, isoleucine, alanine, and phenylalanine. This hydrophobic nature of the active site enabled compounds 10d–f to bind strongly with the enzyme (Figures 5–7). Also, this explains why compounds 10e and 10d had better activity against the enzyme, as they have a more lipophilic phenyl ring than theinyl in compound 10f. Interestingly, compound 10e achieved the highest activity and score, probably due to the methoxy group that forms an additional interaction with the histidine 84 residue. Another aspect worth mentioning is the intramolecular H-bonding between the carbonyl oxygen and the NH functionality in the benzimidazole ring (Figure 8). This bond is thought to be responsible for the stabilization of the active conformation of benzimidazole derivatives 10d–f within the CDK2 kinase active site. All bonding interactions of benzimidazoles 10d–f within CDK2 active site are summarized in Table 5.

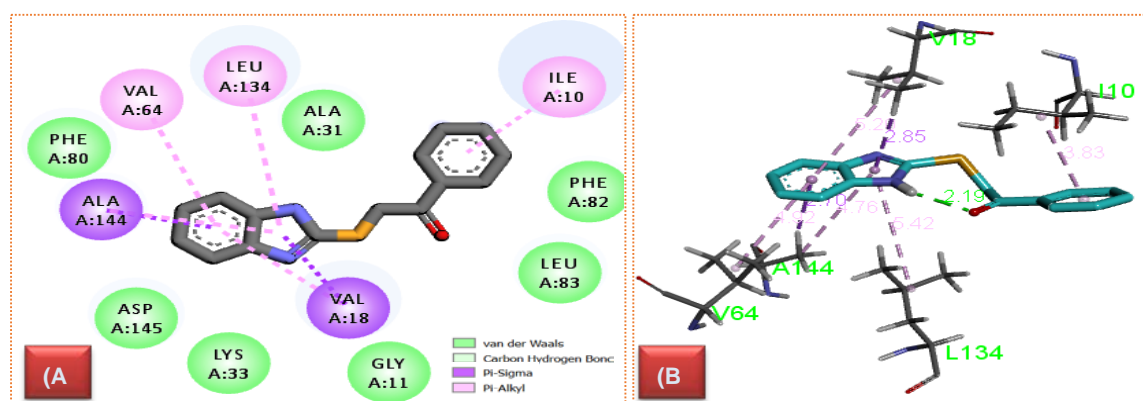


**Figure 5.** (A) 2D and (B) 3D diagram of benzimidazole 10d displaying its interaction within CDK2 kinase active site (distances in Å).

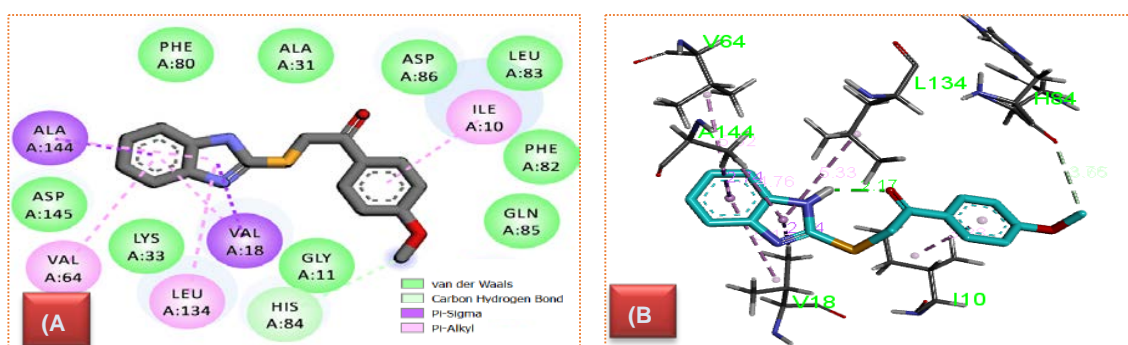


**Figure 6.** (A) 2D and (B) 3D diagram of benzimidazole 10e displaying its interaction within CDK2 kinase active site (distances in Å).

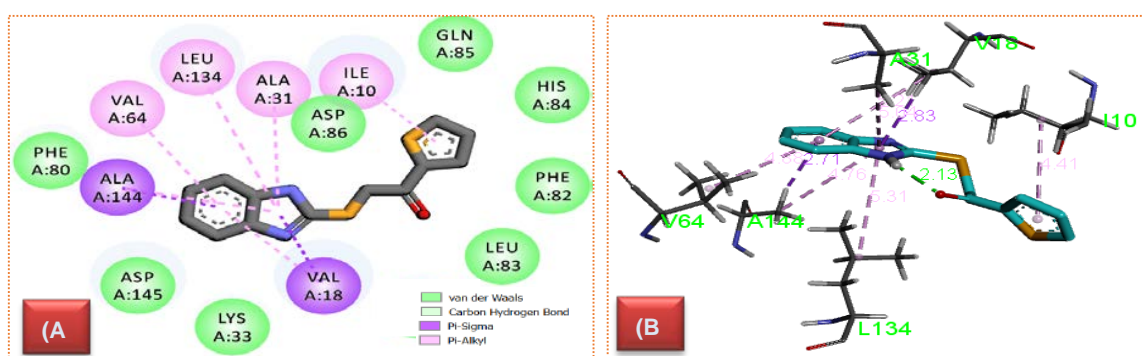


**Figure 7.** (A) 2D and (B) 3D diagram of benzimidazole 10f displaying its interaction within CDK2 kinase active site (distances in Å).

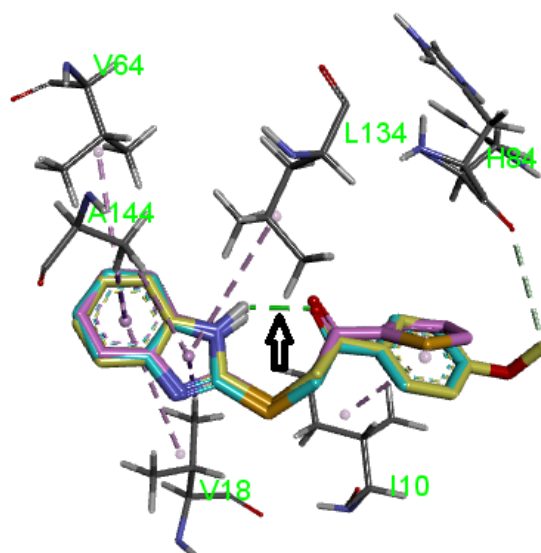


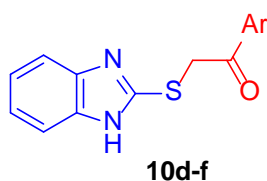
**Figure 8.** The alignment of the docking results, showing very similar orientation of compounds 10d–f, which are stabilized by an intramolecular hydrogen bond, pointed by black arrow. The 10d is in cyan, 10e is in yellow, and 10f is in pink.

**Table 5.** The interaction energy and bonding between benzimidazoles **10d–f** and the CDK2 active site.

Cpd.	Bond Type	Involved Amino Acids	Distance
<b>10d</b>	Pi–Alkyl	Ile10	3.83
	Pi–Sigma	Ala144	2.70
	Pi–Alkyl	Ala144	4.76
	Pi–Alkyl	Leu134	5.42
	Pi–Alkyl	Val64	4.92
	Pi–Alkyl	Val18	5.20
	Pi–Sigma	Val18	2.85
<b>10e</b>	Pi–Alkyl	Ile10	3.88
	Pi–Alkyl	Ala144	4.76
	Pi–Sigma	Ala144	2.47
	Pi–Alkyl	Leu134	5.33
	None Classical hydrogen bond	His84	3.66
	Pi–Alkyl	Val64	5.02
	Pi–Alkyl	Val18	5.13
	Pi–Sigma	Val18	2.84
<b>10f</b>	Pi–Alkyl	Ile10	4.41
	Pi–Alkyl	Val64	4.88
	Pi–Alkyl	Ala144	4.76
	Pi–Sigma	Ala144	2.71
	Pi–Alkyl	Leu134	5.31
	Pi–Alkyl	Ala31	5.04
	Pi–Alkyl	Val18	5.21
	Pi–Sigma	Val18	2.88

#### 2.4.2. In Vitro CDK2 Assay

In this study, benzimidazole derivatives **10d–f** were investigated for their in vitro inhibitory actions against CDK2. The obtained results are presented, as a value ( $IC_{50}$ ), 50% inhibition concentration, in Table 6. The tested benzimidazole derivatives **10d–f** exerted moderate to weak inhibitory action against CDK2, possessing  $IC_{50}$  values equal to 0.89, 0.62, and 1.15  $\mu\text{M}$ , respectively (Table 6). Notably compound **10e**, bearing *para*-methoxy phenyl moiety, was found to be the best CDK2 inhibitor in this study ( $IC_{50} = 0.62 \mu\text{M}$ ), whereas bioisosteric replacement for the phenyl ring with the heteroaryl thiophene ring resulted in compound **10f** with the least CDK2 inhibitory action ( $IC_{50} = 1.15 \mu\text{M}$ ).

**Table 6.**  $IC_{50}$ s for the inhibitory action for benzimidazole derivatives **10d–f** against CDK2.

Cpd.	Ar	$IC_{50}$ ( $\mu\text{M}$ )
		CDK2
<b>10d</b>	$\text{C}_6\text{H}_5$	0.89
<b>10e</b>	4- $\text{CH}_3\text{O}-\text{C}_6\text{H}_4$	0.62
<b>10f</b>	thien-2-yl	1.15

#### 2.5. Pharmacokinetics and Druglikeness Properties' Prediction for Benzimidazoles **10d–f**

Promising candidates should have good pharmacokinetic and pharmacodynamic profiles. Thus, besides determination of the biological activity for benzimidazole derivatives **10d–f**,

their pharmacokinetics, druglikeness, and physicochemical properties were calculated by the SwissADME online tool supplied by the Swiss Institute of Bioinformatics (SIB) [30].

Generally, benzimidazole derivatives 10d–f are predicted to have high GIT absorption. They all are in the human intestinal absorption area in the boiled egg chart [31] (Figure 9). Compound 10e and 10f have no penetration from the Blood Brain Barrier (BBB) and, thus, no central nervous system (CNS) concerns, unlike compound 10d, which has the probability to penetrate the BBB. Also, Figure 9 revealed that they are not a substrate for PGP (P-glyco protein) and so they fit as anticancer agent. In addition, they are not susceptible for efflux by the P-glyco protein transporters found in many types of cancer as a defense mechanism against anticancer drugs.

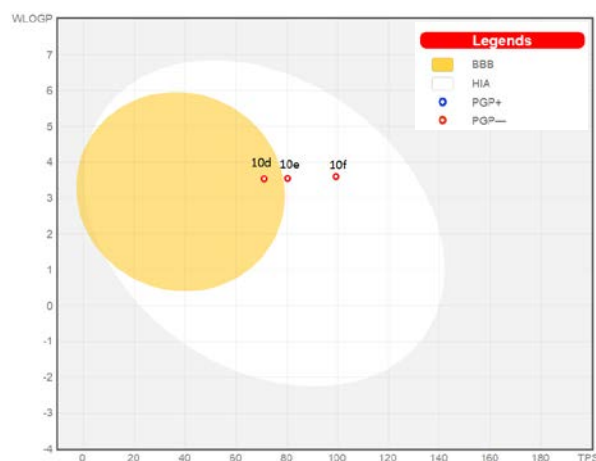


**Figure 9.** Boiled egg chart, generated from SwissADME online web tool, showing the high oral absorption of benzimidazole derivatives, 10d–f, and the probability of compound 10d only to penetrate the BBB.

The bioavailability radar chart explains the high GIT absorption of the three examined compounds 10d–f (Figure 10). The chart contains six critical parameters for oral absorption: FLEX (flexibility), LIPO (lipophilicity), INSATU (saturation), INSOLU (solubility), SIZE, and POLAR (polarity). The chart includes a pink area, representing the optimal range of the six properties, and red lines, representing the predicted physicochemical properties for the explored compounds (Figure 10).

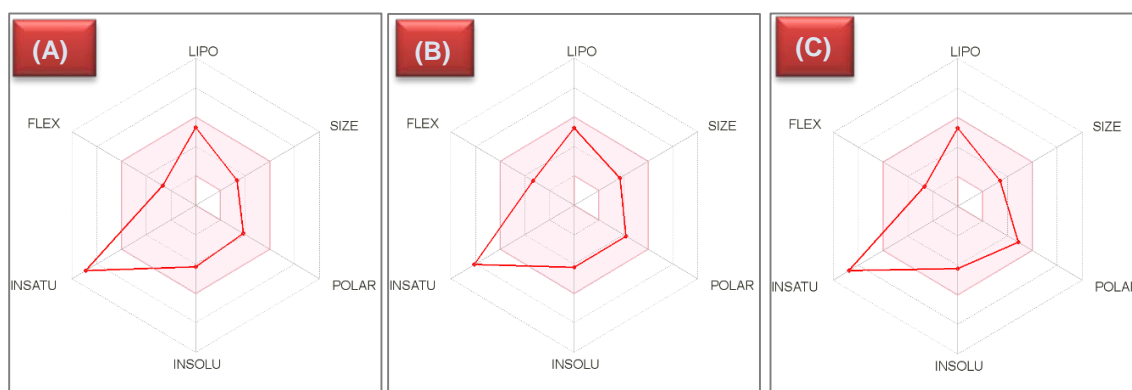


**Figure 10.** Bioavailability radar chart generated by the aid of SwissADME online web tool for benzimidazole derivatives 10d (A), 10e (B), and 10f (C). Pink area is the range for the optimal property values for oral bioavailability, whereas the red line represents benzimidazoles 10d (A), 10e (B), and 10f (C) predicted properties.

The physicochemical properties of the three benzimidazole derivatives 10d–f were located in the desired range of all the parameters except for the saturation. Penetration through the BBB depends on both the  $\text{LOGP}_{o/w}$  and the TPSA (topological polar surface area). The three compounds had  $\text{LOGP}_{o/w}$  between 3.71 and 3.76 but only compound 10d had the suitable TPSA ( $71.05 \text{ \AA}^2$ ) to penetrate the BBB while compounds 10e and 10f had high TPSA values of  $80.28 \text{ \AA}^2$  and  $99.29 \text{ \AA}^2$ , respectively (not suitable for BBB penetration) [32].

The low TPSA value of benzimidazole 10d was due to the nonpolar unsubstituted phenyl ring that was more lipophilic than the theinyl and the methoxy substituted phenyl rings found in compounds 10f and 10e. Compounds 10d–f, as most drugs, were predicted to be metabolized with the liver CYT450 and should be administered alone to minimize the possible drug–drug interactions.

Interestingly, these compounds were found to have no violations in all druglikeness (Veber, Lipinski, Ghose, Muegge, and Egan) rules, and when it comes to medicinal chemistry, all the compounds had neither PAINS (pan assay interference structures) alerts nor structural alerts (Brenks) [33,34]. Table 7 summarizes all the predicted ADME and medicinal chemistry properties for the explored benzimidazole derivatives 10d–f. In conclusion, the three compounds, 10d–f, demonstrated not only good biological activity but also an acceptable ADME and physicochemical properties, especially benzimidazole 10e.

**Table 7.** In silico-predicted ADME and druglikeness properties of benzimidazole derivatives 10d–f.

Cpd.	BBB	GIA	P-gPsubstrate	CYP2C9 Inhibitor	CYP2C19 Inhibitor	CYP1A2 Inhibitor	CYP2D6 Inhibitor	CYP3A4 Inhibitor	PAINS Alerts	Veber Violations	Lipinski Violations
10d	Yes	High	No	Yes	Yes	Yes	Yes	Yes	NO	0	0
10e	No	High	No	Yes	Yes	Yes	Yes	Yes	NO	0	0
10f	No	High	No	Yes	Yes	Yes	No	Yes	NO	0	0

### 3. Materials and Methods

#### 3.1. Chemistry

##### 3.1.1. General

Gallenkamp melting point apparatus was utilized to measure melting points for the herein-prepared imidazole/benzimidazoles derivatives, whereas, the Perkin Elmer FT-IR Spectrum BX apparatus was utilized to record the infrared (IR) spectra, as KBr disks. NMR spectra were recorded on a Bruker NMR spectrometer. The  $^1\text{H}/^{13}\text{C}$  spectra were carried out at 400/100 MHz, respectively, in deuterated dimethylsulfoxide ( $\text{DMSO}-d_6$ ).

##### 3.1.2. General Procedures for Synthesis of Salts 9a–f

To a solution of 2-mercaptoimidazole (1a) or 2-mercaptobenzimidazole (1b) (5 mmol) and the appropriate  $\beta$ -keto ester 5a–c (5 mmol) in glacial acetic acid (10 mL), concentrated sulfuric acid (50 mmol) was added. This reaction mixture was then heated under reflux for one hour, and then allowed to cool to room temperature. The formed precipitate was filtered off, washed with chloroform ( $2 \times 5 \text{ mL}$ ) and then with cold water ( $2 \times 3 \text{ mL}$ ), and dried to yield the corresponding sulfate salts 9a–f, respectively, which were used in the next step without further purification. The spectroscopic data for benzimidazole sulfates 9d–f were in agreement with that previously reported [20].

##### 2-((2-Oxo2-Phenylethyl)thio)1-H-Imidazol3-ium Hydrogen Sulfate (9a)

Pale yellow powder (yield 89%); m.p. 246–248 °C; IR: 3420–3172 (2NH + OH) and 1678 (CO);  $^1\text{H}$  NMR  $\delta$  ppm: 4.69 (s, 2H,  $\text{CH}_2$ ), 7.01–7.05 (m, 2H, H-4 and H-5 of imidazole), 7.50–8.03 (m, 5H, Ar-Hs), 8.34, 10.30, 12.72 (3s, 3H, 2NH + OH).

## 2-((2-(4-Methoxyphenyl)2-Oxoethyl)thio)1-H-Imidazol3-ium Hydrogen Sulfate (9b)

Pale yellow crystals (yield 83%); m.p. 260–262 °C; IR: 3395–3164 (2NH + OH) and 1684 (CO);  $^1\text{H NMR } \delta \text{ ppm}$ : 3.87 (s, 3H,  $-\text{OCH}_3$ ), 4.62 (s, 2H,  $\text{CH}_2$ ), 7.01–7.07 (m, 4H, H-4 and H-5 of imidazole, and H-3 and H-5 of 4- $\text{CH}_3\text{O}-\text{C}_6\text{H}_4$ ), 8.0 (d, 2H, H-2 and H-6 of 4- $\text{CH}_3\text{O}-\text{C}_6\text{H}_4$ ,  $J = 8.8 \text{ Hz}$ ), 8.22, 10.0, 12.75 (3s, 3H, 2NH + OH).

## 2-((2-Oxo2-(Thiophen2-yl)ethyl)thio)1-H-Imidazol3-Ium Hydrogen Sulfate (9c)

White crystals (yield 85%); m.p. 228–230 °C; IR: 3411–3160 (2NH + OH) and 1672 (CO);  $^1\text{H NMR } \delta \text{ ppm}$ : 4.57 (s, 2H,  $\text{CH}_2$ ), 7.01–7.04 (m, 2H, H-4 and H-5 of imidazole), 7.22 (t, 1H, H-4 of thiophene,  $J = 4.4 \text{ Hz}$ ), 7.97 (d, 1H, H-3 of thiophene,  $J = 4.0 \text{ Hz}$ ), 8.02 (d, 1H, H-5 of thiophene,  $J = 4.0 \text{ Hz}$ ), 8.62, 9.43, 12.0 (3s, 3H, 2NH + OH).

## 3.1.3. Procedures for Preparation of Imidazole/Benzimidazol-Based Derivatives 10a–f

To an aqueous solution of sodium hydrogen carbonate, a suspension of the appropriate sulfate salts 9a–f (1 mmol) in water (5 mL) was added. The resulting mixture was allowed to stir at r.t. for three hours. The obtained precipitate was filtered off, washed with cold water ( $3 \times 5 \text{ mL}$ ), dried, and recrystallized from isopropyl alcohol to produce imidazole and benzimidazol derivatives 10a–f, respectively. The spectroscopic data of benzimidazol derivatives 10d–f were in agreement with that previously reported [11].

## 2-((1H-Imidazol2-yl)thio)1-Phenylethan1-One (10a)

White crystals (yield 70%); m.p. 173–175 °C; IR: 3375 (NH) and 1673 (CO);  $^1\text{H NMR } \delta \text{ ppm}$ : 4.69 (s, 2H,  $\text{CH}_2$ ), 7.03–7.05 (m, 2H, H-4 and H-5 of imidazole), 7.54–7.66 (m, 3H, H-3, H-4 and H-5 of  $-\text{C}_6\text{H}_5$ ), 7.98 (d, 2H, H-2 and H-6 of  $-\text{C}_6\text{H}_5$ ,  $J = 6.4 \text{ Hz}$ );  $^{13}\text{C NMR } \delta \text{ ppm}$ : 40.91 ( $\text{CH}_2$ ), 124.32, 128.88 (2C), 129.21 (3C), 133.97, 135.82, 138.42, 194.56 (C=O).

## 2-((1H-Imidazol2-yl)thio)1-(4-Methoxyphenyl)ethan1-One (10b)

White crystals (yield 74%); m.p. 182–184 °C; IR: 3382 (NH) and 1680 (CO);  $^1\text{H NMR } \delta \text{ ppm}$ : 3.86 (s, 2H,  $\text{CH}_2$ ), 4.62 (s, 2H,  $\text{CH}_2$ ), 7.03–7.05 (m, 4H, H-4 and H-5 of imidazole, and H-3 and H-5 of 4- $\text{OCH}_3-\text{C}_6\text{H}_4$ ), 7.98 (d, 2H, H-2 and H-6 of 4- $\text{OCH}_3-\text{C}_6\text{H}_4$ ,  $J = 8.8 \text{ Hz}$ ), 12.18 (s, 1H, NH);  $^{13}\text{C NMR } \delta \text{ ppm}$ : 40.73 ( $\text{CH}_2$ ), 56.05 ( $\text{OCH}_3$ ), 114.42 (3C), 128.65, 130.99 (3C), 138.51, 163.89, 192.95 (C=O).

## 2-((1H-Imidazol2-yl)thio)1-(Thiophen2-yl)ethan1-One (10c)

White crystals (yield 65%); m.p. 147–149 °C; IR: 3405 (NH) and 1679 (CO);  $^1\text{H NMR } \delta \text{ ppm}$ : 4.56 (s, 2H,  $\text{CH}_2$ ), 7.01–7.04 (m, 2H, H-4 and H-5 of imidazole), 7.23 (t, 1H, H-4 of thiophene,  $J = 4.4 \text{ Hz}$ ), 7.97 (d, 1H, H-3 of thiophene,  $J = 4.0 \text{ Hz}$ ), 8.03 (d, 1H, H-5 of thiophene,  $J = 4.4 \text{ Hz}$ ), 12.32 (s, 1H, NH);  $^{13}\text{C NMR } \delta \text{ ppm}$ : 40.60 ( $\text{CH}_2$ ), 129.65 (2C), 134.67 (2C), 135.99, 138.23, 142.63, 187.71 (C=O).

## 3.2. X-ray Crystallographic Analysis

Both imidazole sulfate-salt **9b** and benzimidazole derivative 10f were collected as single crystals via slow evaporation from isopropyl alcohol solutions of each pure derivative at ambient temperature. Data were collected by the use of Bruker APEX-II D8 Venture X-ray diffractometer, which was supported with graphite monochromatic Cu  $K\alpha$  radiation,  $\lambda = 1.54178 \text{ \AA}$  at 296 (2) K, and Mo  $K\alpha$  radiation,  $\lambda = 0.71073 \text{ \AA}$  at 293 (2) K, for imidazole sulfate-salt **9b** and benzimidazole derivative 10f, respectively (Table 8). While the molecular structure for imidazole sulfate-salt **9b** was crystallized in the Triclinic,  $P1$ -,  $a = 9.6682$  (2)  $\text{ \AA}$ ,  $b = 11.9413$  (3)  $\text{ \AA}$ ,  $c = 13.1649$  (3)  $\text{ \AA}$ ,  $\alpha = 93.882$  (2)°,  $\beta = 91.5573$  82 (1)°,  $\gamma = 100$ .(2)°,  $V = 1489.42$  (6)  $\text{ \AA}^3$ ,  $Z = 4$ , benzimidazole derivative 10f was crystallized in the orthorhombic,  $Pbca$ ,  $a = 8.6619$  (2)  $\text{ \AA}$ ,  $b = 9.8244$  (2)  $\text{ \AA}$ ,  $c = 29.7158$  (7)  $\text{ \AA}$ , and  $V = 2528.75$  (10)  $\text{ \AA}^3$ ,  $Z = 8$ . Cell refinements, as well as data reduction, were performed by the use of Bruker SAINT. SHELXT [35,36] was utilized to

solve the structures. The final refinements was performed by the full-matrix, least-squares technique with anisotropic thermal data for nonhydrogen atoms on *F*. CCDC 1524590 and 1429947, comprising the supplementary crystallographic data for imidazole sulfate-salt **9b** and benzimidazole derivative **10f**, were freely available and could be downloaded from the Cambridge Crystallographic Data Centre ([http://www.ccdc.cam.ac.uk/data\\_request/cif](http://www.ccdc.cam.ac.uk/data_request/cif)).

**Table 8.** Experimental details for imidazole sulfate-salt **9b** and benzimidazole derivative **10f**.

Crystal Data	<b>9b</b>	<b>10f</b>
Chemical formula	C <sub>12</sub> H <sub>14</sub> N <sub>2</sub> O <sub>6</sub> S <sub>2</sub>	C <sub>13</sub> H <sub>10</sub> N <sub>2</sub> OS <sub>2</sub>
Mr	346.37	274.35
Temperature (K)	296	293
Crystal system, space group	Triclinic, <i>P1</i> –	Orthorhombic, <i>Pbca</i>
<i>a</i> , <i>b</i> , <i>c</i> (Å)	9.6682 (2), 11.9413 (3), 13.1649 (3)	8.6619 (2), 9.8244 (2), 29.7158 (7)
<i>V</i> (Å <sup>3</sup> )	1489.42 (6)	2528.75 (10)
<i>Z</i>	4	8
$\mu$ (mm <sup>−1</sup> )	3.54	0.41
Radiation type	Cu <i>K</i> $\alpha$	Mo <i>K</i> $\alpha$
Crystal size (mm)	0.60 × 0.16 × 0.12	0.48 × 0.20 × 0.11
<b>Data Collection</b>		
Diffractometer	Bruker APEX-II D8 venture	
Absorption correction	Multi-scan, SADABS Bruker 2014	
T <sub>min</sub> , T <sub>max</sub>	0.226, 0.674	0.89, 0.95
R <sub>int</sub>	0.055	0.038
No. of measured, independent and observed [ <i>I</i> > 2 $\sigma$ ( <i>I</i> )] reflections	16277, 4617, 4132	60453, 4406, 3778
<b>Refinement</b>		
R[ <i>F</i> <sup>2</sup> > 2 $\sigma$ ( <i>F</i> <sup>2</sup> )], wR( <i>F</i> <sup>2</sup> ), <i>S</i>	0.038, 0.105, 1.05	0.039, 0.111, 0.99
Reflections Number	4617	4406
Restraints Number	0	0
Parameters Number	416	167
H atoms treatment	H-atoms were treated by independent and constrained refinement mixture	
$\Delta \rho_{\max}$ , $\Delta \rho_{\min}$ (e Å <sup>−3</sup> )	0.31–0.32	0.52–0.39

### 3.3. Biological Evaluations

Experimental procedures adopted for the cytotoxicity [37] and CDK2 [38] assays were performed as reported earlier, and their details are provided in the supporting materials.

### 3.4. In Silico Studies

#### 3.4.1. Molecular Modeling

Aiming to identify the potential mechanism of action for the most effective anti-proliferative agents (10d–f), the crystal structures of CDK2, CDK4/6, CDK7, and CDK9 were obtained from the (PDB IDs: 5EIV [25], 5I2i [26], 1ua2 [27] and 3lq5 [28], respectively). Docking validity was determined by re-docking the co-crystallized into their complexed enzymes, once in presence of water and another

in water absence. The judgment was based on the calculated RMSD between the docking results and the co-crystallized poses. The docking studies were conducted by Autodock Vina, which demands both receptor and the ligands to be in pdbqt extension thus. M.G.L tools were used to prepare the four enzymes, the co-crystallized and three lead compounds, in the needed format prior to the docking [39]. The obtained docking results were visually inspected by the aid of discovery studio 4.5 visualizer [40]. The selection of the most potential target relied on docking score and interaction within the receptor.

#### 3.4.2. Pharmacokinetics and Druglikeness Properties' Prediction for Benzimidazoles 10d–f

Physicochemical and druglikeness properties for benzimidazole derivatives (10d–f) were predicted by SwissADME server, available online [30].

### 4. Conclusions

This study described an unexpected synthetic route for preparation of 2-((imidazol/benzimidazol2-yl)thio)1-arylethan1-ones 10a–f via reaction of 2-mercaptoimidazole/benzimidazole 2a,b with  $\beta$ -keto esters 6a–c. The structures for compounds 10a–f were unambiguously confirmed based on NMR spectroscopy and single-crystal X-ray crystallographic analyses. X-ray structure crystal analysis was performed for imidazole sulfate-salt 9b and benzimidazole derivative 10f to confirm their structure, and their data were deposited within the CCDC, with deposition numbers CCDC 1524590 and 1429947, respectively. In vitro anticancer activities for herein-reported imidazole/benzimidazoles 10a–f were assessed through a cell-based assay against human breast cancer T4–7D and MCF–7 cell lines. Benzimidazoles 10d–f exerted better anti-proliferative action towards T4–7D and MCF–7 cell lines than their corresponding imidazole counterparts, 10a–c. Furthermore, CDK2 kinase was suggested as a potential enzymatic target for benzimidazoles 10d–f. The obtained results from the in vitro CDK2 assay revealed that compounds 10d–f possess good inhibitory action against CDK2 with  $IC_{50}$ s of 0.89, 0.62, and 1.15  $\mu$ M, respectively. Besides, the molecular docking study investigated the possible binding pattern and interactions for benzimidazoles 10d–f within CDK2 active site. Finally, several key ADME and druglikeness properties were estimated by the SwissADME online tool. Interestingly, benzimidazoles 10d–f were found to have no violations in all druglikeness (Veber, Lipinski, Ghose, Muegge, and Egan) rules. In addition, they had neither PAINS nor structural alerts (Brenks). In conclusion, benzimidazoles 10d–f demonstrated not only promising anticancer activities but also an acceptable ADME and physicochemical properties, especially benzimidazole 10e.

**Supplementary Materials:** Supplementary materials are available online at <http://www.mdpi.com/2073-4352/10/6/446/s1>.

**Author Contributions:** The manuscript was written through contributions of all authors. All authors have given approval to the final version of the manuscript.

**Funding:** The authors extend their appreciation to the Deanship of Scientific Research at Princess Nourah bint Abdulrahman University for funding this work through the Research Groups Program Grant No. RGP-1440-0025.

**Conflicts of Interest:** The authors declare no conflict of interest.

### References

1. Yadav, G.; Ganguly, S. Structure activity relationship (SAR) study of benzimidazole scaffold for different biological activities: A mini-review. *Eur. J. Med. Chem.* **2015**, *97*, 419–443. [[CrossRef](#)] [[PubMed](#)]
2. Akhtar, W.; Khan, M.F.; Verma, G.; Shaquiquzzaman, M.; Rizvi, M.A.; Mehdi, S.H.; Akhter, M.; Alam, M.M. Therapeutic evolution of benzimidazole derivatives in the last quinquennial period. *Eur. J. Med. Chem.* **2016**, *126*, 705–753. [[CrossRef](#)] [[PubMed](#)]
3. Tahlan, S.; Kumar, S.; Narasimhan, B. Pharmacological significance of heterocyclic 1H-benzimidazole scaffolds: A review. *BMC Chem.* **2019**, *13*, 101. [[CrossRef](#)] [[PubMed](#)]
4. Gaba, M.; Mohan, C. Development of drugs based on imidazole and benzimidazole bioactive heterocycles: Recent advances and future directions. *Med. Chem. Res.* **2016**, *25*, 173–210. [[CrossRef](#)]

5. Bräse, S. *Privileged Scaffolds in Medicinal Chemistry: Design, Synthesis, Evaluation*; Royal Society of Chemistry: Cambridge, UK, 2015; Chapter 2; pp. 98–113, ISBN 9781–7–82620–303.
6. Ali, I.; Lone, M.N.; Aboul-Enein, H.Y. Imidazoles as potential anticancer agents. *MedChemComm* **2017**, *8*, 1742–1773. [[CrossRef](#)]
7. Shrivastava, N.; Naim, M.J.; Alam, M.J.; Nawaz, F.; Ahmed, S.; Alam, O. Benzimidazole scaffold as anticancer agent: Synthetic approaches and structure–activity relationship. *Arch. Pharm.* **2017**, *350*, e201700040. [[CrossRef](#)]
8. Tahlan, S.; Kumar, S.; Kakkar, S.; Narasimhan, B. Benzimidazole scaffolds as promising antiproliferative agents: A review. *BMC Chem.* **2019**, *13*, 66. [[CrossRef](#)]
9. Yadav, S.; Narasimhan, B. Perspectives of benzimidazole derivatives as anticancer agents in the new era. *Anticancer Agents Med. Chem.* **2016**, *16*, 1403–1425. [[CrossRef](#)]
10. Akhtar, M.J.; Yar, M.S.; Sharma, V.K.; Khan, A.A.; Ali, Z.; Haider, M.R.; Pathak, A. Recent Progress of Benzimidazole Hybrids for Anticancer Potential. *Curr. Med. Chem.* **2019**. [[CrossRef](#)]
11. Aniket, P.; Shantanu, D.S.; Anagha, O.B.; Ajinkya, P.S. Iodine catalyzed convenient synthesis of 2-aryl1-arylmethyl1-H-benzimidazoles in aqueous media. *Int. J. ChemTech Res.* **2015**, *8*, 496–500.
12. Wan, J.P.; Gan, S.F.; Wu, J.M.; Pan, Y. Water mediated chemoselective synthesis of 1,2-disubstituted benzimidazoles using o-phenylenediamine and the extended synthesis of quinoxalines. *Green Chem.* **2009**, *11*, 1633–1637. [[CrossRef](#)]
13. Di Gioia, M.L.; Cassano, R.; Costanzo, P.; Herrera Cano, N.; Maiuolo, L.; Nardi, M.; Nicoletta, F.P.; Oliverio, M.; Procopio, A. Green synthesis of privileged benzimidazole scaffolds using active deep eutectic solvent. *Molecules* **2019**, *24*, 2885. [[CrossRef](#)]
14. Herrera Cano, N.; Uranga, J.G.; Nardi, M.; Procopio, A.; Wunderlin, D.A.; Santiago, A.N. Selective and eco-friendly procedures for the synthesis of benzimidazole derivatives. The role of the Er(OTf)<sub>3</sub> catalyst in the reaction selectivity. *Beilstein J. Org. Chem.* **2016**, *12*, 2410–2419. [[CrossRef](#)] [[PubMed](#)]
15. Sapkal, S.B.; Shelke, K.F.; Sonar, S.S.; Shingate, B.B.; Shingare, M.S. Acidic ionic liquid catalyzed environmentally friendly synthesis of benzimidazole derivatives. *Bull. Catal. Soc. India* **2009**, *2*, 78–83.
16. Sharma, J.; Soni, P.K.; Bansal, R.; Halve, A.K. Synthetic Approaches Towards Benzimidazoles by the Reaction of o-Phenylenediamine with Aldehydes Using a Variety of Catalysts: A Review. *Curr. Org. Chem.* **2018**, *22*, 2280–2299. [[CrossRef](#)]
17. Brain, C.T.; Brunton, S.A. An intramolecular palladium-catalysed aryl amination reaction to produce benzimidazoles. *Tetrahedron Lett.* **2002**, *43*, 1893–1895. [[CrossRef](#)]
18. Nale, D.B.; Bhanage, B.M. The use of various o-phenylenediamines and N-substituted formamides as C 1 sources in a zinc-catalyzed cyclization in the presence of poly (methylhydrosiloxane) provides benzimidazoles in good yields. Benzoxazole and benzothiazole derivates can also be synthesized. *Synlett* **2015**, *26*, 2831–2834.
19. Mahesh, D.; Sadhu, P.; Punniyamurthy, T. Copper (II)-catalyzed oxidative cross-coupling of anilines, primary alkyl amines, and sodium azide using TBHP: A route to 2-substituted benzimidazoles. *J. Org. Chem.* **2016**, *81*, 3227–3234. [[CrossRef](#)]
20. Abdel-Aziz, H.A.; Ghabbour, H.A.; Eldehna, W.M.; Al-Rashood, S.T.; Al-Rashood, K.A.; Fun, H.K.; Al-Tahhan, M.; Al-Dhfyhan, A. 2-((Benzimidazol-2-yl) thio)-1-arylethan-1-ones: Synthesis, crystal study and cancer stem cells CD133 targeting potential. *Eur. J. Med. Chem.* **2015**, *104*, 1–10. [[CrossRef](#)]
21. Abdel-Aziz, H.A.; Eldehna, W.M.; Ghabbour, H.; Al-Ansary, G.H.; Assaf, A.M.; Al-Dhfyhan, A. Synthesis, crystal study, and anti-proliferative activity of some 2-benzimidazolylthioacetophenones towards triple-negative breast cancer MDA-MB4–68 cells as apoptosis-inducing agents. *Int. J. Mol. Sci.* **2016**, *17*, 1221. [[CrossRef](#)]
22. Al-Ansary, G.H.; Eldehna, W.M.; Ghabbour, H.A.; Al-Rashood, S.T.; Al-Rashood, K.A.; Eladwy, R.A.; Al-Dhfyhan, A.; Kabil, M.M.; Abdel-Aziz, H.A. Cancer stem cells CD133 inhibition and cytotoxicity of certain 3-phenylthiazolo [3,2-*a*]benzimidazoles: Design, direct synthesis, crystal study and in vitro biological evaluation. *J. Enzym. Inhib. Med. Chem.* **2017**, *32*, 986–991. [[CrossRef](#)] [[PubMed](#)]
23. Allen, F.H.; Kennard, O.; Watson, D.G.; Brammer, L.; Orpen, A.G.; Taylor, R. Tables of bond lengths determined by X-ray and neutron diffraction. Part 1. Bond lengths in organic compounds. *J. Chem. Soc. Perkins Trans. 2* **1987**, *12*, S1–S19. [[CrossRef](#)]
24. Skehan, P.; Storeng, R.; Scudiero, D. New colorimetric cyto-toxicity assay for anticancer-drug screening. *J. Natl. Cancer Inst.* **1990**, *82*, 1107–1112. [[CrossRef](#)] [[PubMed](#)]

25. Ayaz, P.; Andres, D.; Kwiatkowski, D.A.; Kolbe, C.C.; Lienau, P.; Siemeister, G.; Lucking, U.; Stegmann, C.M. Conformational Adaptation May Explain the Slow Dissociation Kinetics of Roniciclib (BAY 1000394), a Type I CDK Inhibitor with Kinetic Selectivity for CDK2 and CDK9. *ACS Chem. Biol.* **2016**, *11*, 1710–1719. [[CrossRef](#)]
26. Chen, P.; Lee, N.V.; Hu, W.; Xu, M.; Ferre, R.A.; Lam, H.; Bergqvist, S.; Solowiej, J.; Diehl, W.; He, Y.A.; et al. Spectrum and Degree of CDK Drug Interactions Predicts Clinical Performance. *Mol. Cancer Ther.* **2016**, *15*, 2273–2281. [[CrossRef](#)]
27. Lolli, G.; Lowe, E.D.; Brown, N.R.; Johnson, L.N. The Crystal Structure of Human CDK7 and Its Protein Recognition Properties. *Structure* **2004**, *12*, 2067–2079. [[CrossRef](#)]
28. Bettayeb, K.; Baunbak, D.; Delehouze, C.; Loaec, N.; Hole, A.J.; Baumli, S.; Endicott, J.A.; Douc-Rasy, S.; Benard, J.; Oumata, N.; et al. CDK Inhibitors Roscovitine and CR8 Trigger Mcl1– Down-Regulation and Apoptotic Cell Death in Neuroblastoma Cells. *Genes Cancer* **2010**, *1*, 369–380. [[CrossRef](#)]
29. Wei, Y.; Li, J.; Qing, J.; Huang, M.; Wu, M.; Gao, F.; Lin, J. Discovery of novel hepatitis C virus NS5B polymerase inhibitors by combining random forest, multiple e-pharmacophore modeling and docking. *PLoS ONE* **2016**, *11*, e0148181. [[CrossRef](#)]
30. Daina, A.; Michielin, O.; Zoete, V. SwissADME: A free web tool to evaluate pharmacokinetics, drug-likeness and medicinal chemistry friendliness of small molecules. *Sci. Rep.* **2017**, *7*, 42717. [[CrossRef](#)]
31. Daina, A.; Zoete, V. A BOILED-Egg to predict gastrointestinal absorption and brain penetration of small molecules. *ChemMedChem* **2016**, *11*, 1117–1121. [[CrossRef](#)]
32. Ertl, P.; Rohde, B.; Selzer, P. Fast Calculation of Molecular Polar Surface Area as a Sum of Fragment-Based Contributions and Its Application to the Prediction of Drug Transport Properties. *J. Med. Chem.* **2000**, *43*, 3714–3717. [[CrossRef](#)] [[PubMed](#)]
33. Baell, J.B.; Holloway, G.A. New substructure filters for removal of pan assay interference compounds (PAINS) from screening libraries and for their exclusion in bioassays. *J. Med. Chem.* **2010**, *53*, 2719–2740. [[CrossRef](#)] [[PubMed](#)]
34. Veber, D.F.; Johnson, S.R.; Cheng, H.Y.; Smith, B.R.; Ward, K.W.; Kopple, K.D. Molecular properties that influence the oral bioavailability of drug candidates. *J. Med. Chem.* **2002**, *45*, 2615–2623. [[CrossRef](#)] [[PubMed](#)]
35. Sheldrick, G.M. A short history of SHELX. *Acta Crystallogr. Sect. A* **2008**, *64*, 112–122. [[CrossRef](#)]
36. Sheldrick, G.M. *SHELXTL-PC (Version 5.1)*; Siemens Analytical Instruments, Inc.: Madison, WI, USA, 1997.
37. Sabt, A.; Abdelhafez, O.M.; El-Haggag, R.S.; Madkour, H.M.; Eldehna, W.M.; El-Khrisy, E.E.D.A.; Abdel-Rahman, M.A.; Rashed, L.A. Novel coumarin-6-sulfonamides as apoptotic anti-proliferative agents: Synthesis, *in vitro* biological evaluation, and QSAR studies. *J. Enzym. Inhib. Med. Chem.* **2018**, *33*, 1095–1107. [[CrossRef](#)]
38. Said, M.A.; Eldehna, W.M.; Nocentini, A.; Fahim, S.H.; Bonardi, A.; Elgazar, A.A.; Kryštof, V.; Soliman, D.H.; Abdel-Aziz, H.A.; Gratteri, P.; et al. Sulfonamide-based ring-fused analogues for CAN508 as novel carbonic anhydrase inhibitors endowed with antitumor activity: Design, synthesis, and *in vitro* biological evaluation. *Eur. J. Med. Chem.* **2020**, *189*, 112019. [[CrossRef](#)]
39. Trott, O.; Olson, A.J. AutoDock Vina: Improving the speed and accuracy of docking with a new scoring function, efficient optimization and multithreading. *J. Comp. Chem.* **2010**, *31*, 455–461. [[CrossRef](#)]
40. Available online: <https://3dsbiovia.com/resource-center/downloads/> (accessed on 6 March 2020).

